# Simulating the dispensing of complex rheological fluids on arbitrary geometries using the immersed boundary method

Simon Ingelsten[1], Johan Göhl[1], Andreas Mark[1] and Fredrik Edelvik[1]
[1] Fraunhofer-Chalmers Research Centre for Industrial Mathematics, 412 88 Gothenburg, Sweden

## ABSTRACT

A numerical framework to simulate dispensing of fluids with different types of complex rheology is presented. The framework is based on an incompressible flow solver that uses immersed boundary methods and an automatically generated octree grid. It therefore supports simulation with arbitrary geometry and of moving application with various injection models with minimum setup time. The framework also supports rheology models spanning from purely viscous models to more advanced viscoelastic stress models.

Three examples of applications are given, namely for seam sealing in automotive bodies, swirled adhesive extrusion and wire fed additive manufacturing of metal. The wide range of applications shows the potential of the framework and indicates that many more possible applications are conceivable.

## INTRODUCTION

Processes that include dispensing of fluids with complex rheology are common in various types of industrial applications, e.g. seam sealing application in automotive bodies, adhesive extrusion and additive manufacturing. As the demand for tools to simulate and predict the outcome of the processes increases, so does the need for robust and efficient numerical frameworks and models that accurately describe the specific features of such flows. In this paper such a framework is presented.

The simulation framework is based on IPS IBOFlow®, an incompressible finite volume flow solver developed at the Fraunhofer-Chalmers Research Centre for Industrial Mathematics in Gothenborg, Sweden. The solver has previously been used to simulate conjugate heat transfer[10], fluid-structure interaction[12] and two-phase flows with shear thinning fluids for seam sealing[11, 13, 15] and adhesive extrusion[14].

For the flows in consideration, four common main properties can be identified,

1. Two-phase flow of the applied material and the surrounding air
2. Moving application along a prescribed path
3. Arbitrary substrate geometry
4. Non-Newtonian material rheology

All these properties require careful modelling in order to correctly account for them in simulations.

Since non-Newtonian fluid flow is considered, a subject of importance is of course the rheology model. For flow of viscoelastic fluids it may be sufficient to use a purely viscous model such as the Carreau model[7], especially if the flow is dominated by inertia. For flows dominated by elasticity, however, the accuracy of such models are often insufficient as they lack the ability to store elastic energy. For such flows the proper approach is to instead use a constitutive model that describes the transient evolution of the viscoelastic stress tensor. A wide range of viscoelastic constitutive models can be found in the literature, ranging from simpler linear models such as the Upper-Convected Maxwell (UCM) and Oldroyd-B models[2] and more physically accurate nonlinear models such as the Phan Thien Tanner (PTT) model[1] and the Finitely Extensible Nonlinear Elasticity (FENE) models[3]. The main improvement of the nonlinear models compared to the linear models is that they prevent unbounded normal stresses by limiting the extension of the polymers in the viscoelastic fluid.

Another type of rheology that is considered in this paper is temperature-dependent viscosity. This is typically relevant for e.g. liquid metal flow.

The aim of this work is to present the building blocks of a numerical framework for simulating the flows discussed above and highlight some example applications. The rest of the paper is structured as follows. First the governing equations are defined, then the numerical method is described. Finally three example applications are shown and some conclusions are drawn. The examples are application of seam sealing in automotive bodies, swirled extrusion of adhesive and wire fed additive manufacturing of metal.

## GOVERNING EQUATIONS

The non-Newtonian fluid flow is described be the incompressible momentum and continuity equations

$$\rho \frac{\partial \mathbf{u}}{\partial t} + \rho \mathbf{u} \cdot \nabla \mathbf{u} = -\nabla p + \nabla \cdot \sigma + \mathbf{f}, \tag{1}$$

$$\nabla \cdot \mathbf{u} = 0, \tag{2}$$

where $\rho$ is fluid density, $\mathbf{u}$ velocity, $p$ pressure, $\tau$ the deviatoric stress and $\mathbf{f}$ a body force. The deviatoric stress is divided into a purely viscous part and a viscoelastic stress as

$$\tau = 2\mu \mathbf{S} + \tau_v, \tag{3}$$

where $\mu$ is viscosity, $\mathbf{S}$ the rate of strain

$$\mathbf{S} = \frac{1}{2}\left(\nabla \mathbf{u} + (\nabla \mathbf{u})^T\right), \tag{4}$$

and $\tau_v$ the viscoelastic stress.

The non-Newtonian rheology models are divided into two main categories. The first consists of purely viscous fluids, for which $\tau_v \equiv 0$ and $\mu > 0$ is a function of the local state of the flow. Two such models are considered, one being the Carreau model, reading[7]

$$\mu(\dot{\gamma}) = \mu_\infty + (\mu_0 - \mu_\infty)\left(1 + (\xi \dot{\gamma})^2\right)^{\frac{n-1}{2}}, \tag{5}$$

where $\dot{\gamma} = |\mathbf{S}|$ is the local shear rate, $\mu_\infty$ and $\mu_0$ the viscosities at zero and infinite shear rate, respectively, $\xi$ is a characteristic time and $n$ a power law index. The other viscous model considered is the temperature dependent viscosity for liquid metals and alloys calculated as[9]

$$\mu(T) = \mu_0^T \exp\left(-\frac{E_A}{RT}\right), \tag{6}$$

where $T$ is the local temperature, $\mu_0^T$ a viscosity constant, $E_A$ the activation energy and R the ideal gas constant. In this case the temperature is described by the heat transport equation.

$$\frac{\partial T}{\partial t} + \mathbf{u} \cdot \nabla T = \nabla \cdot \left(\frac{k_T}{\rho c_p} \nabla T\right) + S_T, \tag{7}$$

where $k_T$ is thermal conductivity, $c_p$ heat capacity and $S_T$ a source term.

The second main type of rheology model consists of the viscoelastic models, for which $\mu \geq 0$ is constant and $\tau_v$ is described by a constitutive equation. In this work the linear form of the Phan-Thien-Tanner (PTT) model is used, reading

$$\lambda \overset{\triangledown}{\tau}_v + \left(1 + \frac{\varepsilon \lambda}{\eta} \mathrm{Tr}(\tau_v)\right) \tau_v = 2\eta \mathbf{S}, \tag{8}$$

where $\mathrm{Tr}(\tau_v)$ denotes the trace of $\tau_v$ and $\overset{\triangledown}{\tau}_v$ is the upper convected derivative

$$\overset{\triangledown}{\tau} = \frac{d\tau}{dt} - \nabla \mathbf{u}^T \cdot \tau - \tau \cdot \nabla \mathbf{u}, \tag{9}$$

where $d/dt$ denotes the material time derivative.

The two-phase flow of the non-Newtonian fluid and the surrounding air is modelled with the Volume of Fluid (VOF) method. A single set of momentum and continuity equations is then used for the whole domain and the respective phases are described by the local volume fraction $\alpha \in [0,1]$. In areas where only air is present $\alpha = 1$ and in areas where only the non-Newtonian fluid is present $\alpha = 0$. A location where $0 < \alpha < 1$ lies on the interface between the phases. Local properties in the flow, e.g. density or viscosity, are calculated as

$$\phi = \alpha\phi_{\text{air}} + (1-\alpha)\phi_{\text{NN}}, \tag{10}$$

where $\phi_{\text{air}}$ is the property of the air and $\phi_{\text{NN}}$ that of the non-Newtonian fluid. The evolution of $\alpha$ is described by the advection equation

$$\frac{\partial \alpha}{\partial t} + \mathbf{u}\cdot\nabla\alpha = 0. \tag{11}$$

NUMERICAL METHOD

The simulations are performed with IPS IBOFlow®, which is an incompressible flow solver. The key feature of the solver is the use of immersed boundary methods in combination with an octree grid that is automatically generated and dynamically refined near objects and interfaces. Finite volume discretization of (1), (2), (7) and (11) is carried out on the octree grid, and the SIMPLEC algorithm is used to couple pressure and momentum. In each time step the following steps are performed:

1. Calculate non-Newtonian stresses ($\mu$ or $\tau$)
2. Solve (1) and (2) iteratively for $\mathbf{u}$ and p.
3. Solve (11) for $\alpha$
4. Solve additional equations (e.g. for $T$)

Boundary conditions from interior objects in the computational domain are treated using the mirroring immersed boundary method[6,8]. The velocity field is then implicitly mirrored across the boundary surface, such that the resulting velocity at the surface satisfies the boundary condition for the converged solution. There is therefore no need for a boundary fitted grid. The combination with the automatically generated octree grid is therefore highly efficient for simulation of flow with arbitrary boundary geometry and moving free surfaces.

Extra care needs to be taken for the discretization of (11) for $\alpha$. Since the equation includes no natural diffusion, it is important to minimize the introduction of numerical diffusion in order to maintain a sharp interface between the phases. The compact CICSAM scheme[4] is therefore used.

An injection model is used to describe the application of material with a nozzle moving along a predefined path. The injection step can be summarized in two main parts:

1. Refine octree grid in the neighbourhood of injection.
2. Identify injection cells and add material by changing $\alpha$ and setting the velocity.

The velocity in the injection cells is set to

$$u_{\text{inj}} = u_{\text{flow}} + u_{\text{app}}, \tag{12}$$

where $u_{\text{flow}}$ is the injection velocity based on the material flow rate and $u_{\text{app}}$ the velocity of the applicator. Due to possible geometry discrepancies between the real nozzle shape and the injection cells, a correction step is used to control the inlet flow. In each time step the total volume of injected material in the domain is calculated. A flow rate correction is then calculated as

$$\dot{V}_{\text{corr}} = \max\left(\xi_s \frac{V_{\text{tot}} - V_{\text{tot,nom}}}{\Delta t}, \xi_l \dot{V}_{\text{nom}}\right), \tag{13}$$

where $\xi_s \in (0,1]$ is introduced to give smooth flow variations and $\xi_l \in [0,1)$ enforces a lower limit relative to the nominal flow rate. $V_{\text{tot}}$ is the calculated volume, $V_{\text{tot,nom}}$ the nominal total volume, $\dot{V}_{\text{nom}}$ the nominal flow rate and $\Delta t$ the fluid time step. The volume flow rate for the injection is then calculated as

$$\dot{V} = \xi_r(\dot{V}_{\text{nom}} + \dot{V}_{\text{corr}}) + (1-\xi_r)\dot{V}_{\text{old}}, \tag{14}$$

where $\xi_r \in (0,1)$ is a relaxation factor and $\dot{V}_{\text{old}}$ is the flow rate used in the previous time step.

A geometrical model is used to determine the injection cells. The models depend on the type of dispensing application, but can be divided in two main categories:

- Direct injection.
- Projected injection.

In the direct injection approach the material is injected at the nozzle opening and the geometrical shape of the nozzle directly determines the injection cells. In Figure 1 an example is shown of the injection cells for a circular adhesive nozzle. The octree discretization with refinements are also shown along with the bead, which is visualized with the contour surface $\alpha = 1/2$.

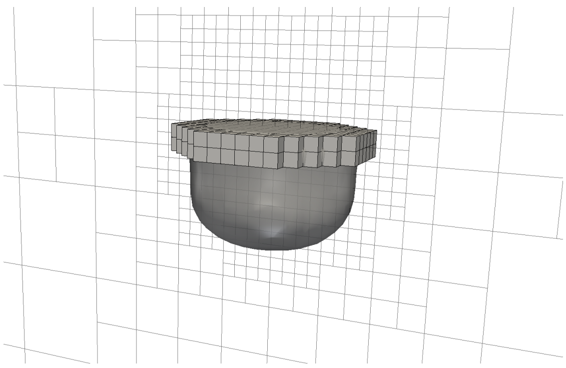

Figure 1. Injection cells (solid cubes) for a circular nozzle model.

The projected injection approach relies on the assumption that the flow of material from the nozzle to the target surface has a large stokes number, such that the effect of the surrounding air is negligible. The simulation of this part of the application may then be replaced by a projection model. Injection is then instead performed at the target surface, which significantly reduces the computational effort. For more details, the reader is referred to[13].

The non-Newtonian stresses are calculated from the flow field. For the purely viscous models the local viscosity is calculated directly from the velocity field using (5) or from the temperature field using (6), depending on which model is being used.

For the viscoelastic fluids, the constitutive equation must be solved and the resulting stresses must be coupled to the fluid momentum equation. For this, a novel Lagrangian-Eulerian method is used, in which the viscoelastic stresses are solved and stored in a Lagrangian node set that is convected by the fluid and the stresses are interpolated to the Eulerian fluid grid using radial basis functions (RBF). The approach is motivated by the lack of natural diffusion in most viscoelastic constitutive equations. The Lagrangian frame also provides a natural description to transport the stresses resulting from the deformation history of fluid elements. An illustration of the concept can be seen in Figure 2.

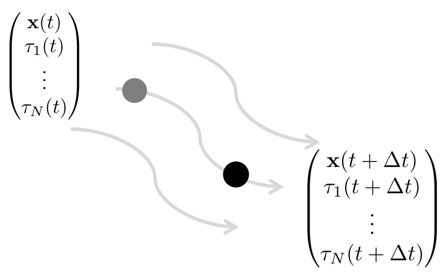


Figure 2. Sketch of stresses convected in a Lagrangian node.

In each node the updated position and stress are obtained by solving the system of ordinary differential equations

$$\begin{cases} \dot{\mathbf{x}} &= \mathbf{u} \\ \dot{\tau}_v &= G(\tau_v, \nabla \mathbf{u}) \end{cases}, \tag{15}$$

where $(\dot{\bullet})$ denotes time derivative and the right hand side $G(\tau_v, \nabla \mathbf{u})$ follows directly from (8). The local properties needed for solving the system, i.e. $\mathbf{u}$ and $\nabla \mathbf{u}$, are interpolated from the octree grid to the current position of the node. When (15) is solved and the updated stresses are available in the Lagrangian nodes, the stresses are interpolated to the cell centers of the Eulerian fluid grid using RBF. An interpolant $\hat{f}(\mathbf{x})$ of a function $f(\mathbf{x})$ that is known in a finite set of points is then calculated as the weighted sum[5]

$$\hat{f}(\mathbf{x}) = \sum_{i=1}^{N} w_i \phi(|\mathbf{x} - \mathbf{x}_i|), \tag{16}$$

where $\mathbf{x}_i$ are the points where $f$ is known, $w_i$ the corresponding weights, $N$ the number of points and $\phi(r)$ the RBF. The weights are determined by solving the linear system implied by the constraint that the interpolant should be exact where $f$ is known, i.e. $\hat{f}(\mathbf{x}_i) = f(\mathbf{x}_i) \quad \forall i = 1, \ldots, N$. This gives

$$A\mathbf{w} = \mathbf{f}, \tag{17}$$

where

$$A_{ij} = \phi(|\mathbf{x}_i - \mathbf{x}_j|), \tag{18}$$

$$\mathbf{w} = [w_i \cdots w_N]^T, \tag{19}$$

$$\mathbf{f} = [f(\mathbf{x}_i) \cdots f(\mathbf{x}_N)]^T. \tag{20}$$

When the components of $\tau_v$ are known in the cell centers they are integrated over the cells using Gauss's divergence theorem as

$$\int_{\text{cell}} \nabla \cdot \tau dV = \sum_f A_f \hat{\mathbf{n}}_f \cdot \tau_f, \tag{21}$$

where the sum is taken over the cell faces and $A_f$, $\hat{\mathbf{n}}_f$ and $\tau_{v,f}$ are the area, normal vector and stress tensor at the respective faces.

## RESULTS

In this section, three example applications are presented. The examples cover the rheology models and injection model approaches described above.

The first example considers flat bead seam sealing, which is applied in automotive bodies to cover holes and cavities to prevent corrosion. The rheology of the shear thinning sealant is described with the Carreau model with parameters $\mu_0 = 264.76\,\text{Pas}$, $\mu_\infty = 3.096\,\text{Pas}$, $\xi = 0.4796\,\text{s}$ and $n = 0.45359$. The parameters are determined by fitting the viscosity resulting from (5) to data from a rheometer shear sweep. The projected injection approach is used to describe the input of material into the computational domain. The flow exiting the sealing nozzle consists of a thin bead, where the width is a function of the distance from the nozzle and the flow rate. The injection model is constructed by measuring the width at varying distance for a range of flow rates relevant for the process. The data is used in the simulations to reconstruct the bead and predict the impact at the target surface with ray tracing. In Figure 3 an experimental bead and the corresponding reconstructed bead from a simulation is shown.

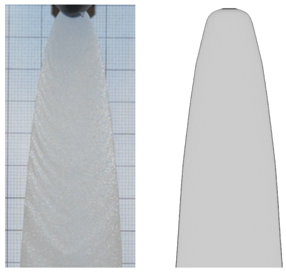

Figure 3. Experiment (left) and reconstruction in simulation (right) of the sealing bead in the air.

A set of beads in the floor of a Scania truck cab are simulated. The corresponding real beads are 3D-scanned to enable comparison between the scanned and the simulated beads, respectively. In Figure 4 an overview is shown of the scanned truck floor and sealing beads. The flow rates used to apply the beads vary between 15 ml/s and 35 ml/s and the movement speed of the applicator is around 0.3 m/s to 0.5 m/s

In Figure 5 the simulated and scanned beads, respectively, are shown in an area of the truck floor. The bead passes a corner and includes an area with a thick sealant layer. High flow rates and thick layers of sealant typically increases the computational complexity of the problem. It is observed, however, that the simulation gives an accurate prediction of the real bead in this case.

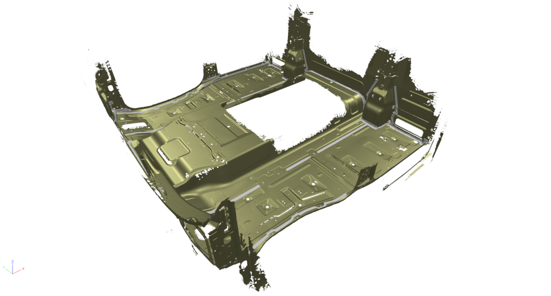

Figure 4. Scanned sealing beads in truck floor.

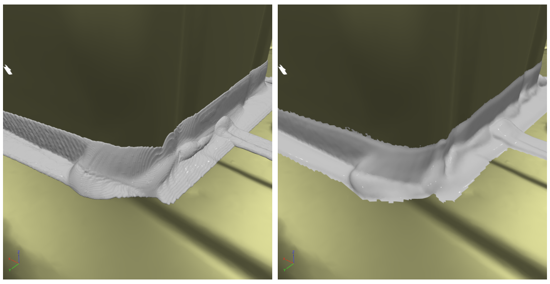

Figure 5. Simulated (left) and scanned (right) sealing bead in the Scania truck.

In Figure 6 a similar visual comparison between the simulated and scanned beads is shown in an area where the bead is applied on a vertical wall. This causes the sealant to flow downwards along the wall before finally sticking. The simulation captures the geometrical features resulting from this scenario.

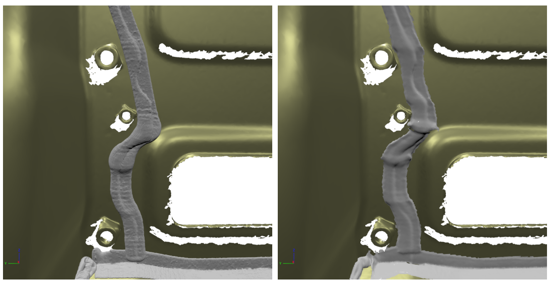

Figure 6. Simulated (left) and scanned (right) sealing bead in the Scania truck.

A detailed comparison of the bead cross section is performed in a relevant area for the beads. The positions are defined in Figure 7. In Figure 8 the comparisons in the cross sections are shown. The results show that the simulations are in good agreement with the scanned data in the studied areas.

The second example is of extrusion of adhesive material with a swirled nozzle. In this type of application a very small circular nozzle rotates with high speed, forming a thread-like spiral shaped bead in the air. The flow exhibits a significant degree of elasticity, and the viscoelastic PTT model is therefore used to model the adhesive rheology. The parameters $\lambda = 0.0821\,\mathrm{s}$, $\eta = 3065\,\mathrm{Pas}$ and $\varepsilon = 0.5$ and $\mu = 60\,\mathrm{Pas}$ are determined using rheometer data from a shear sweep and an oscillating frequency sweep.

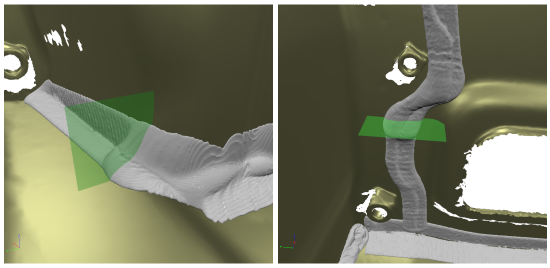

Figure 7. Cross sections (green planes) used for detailed comparison of the sealing beads.

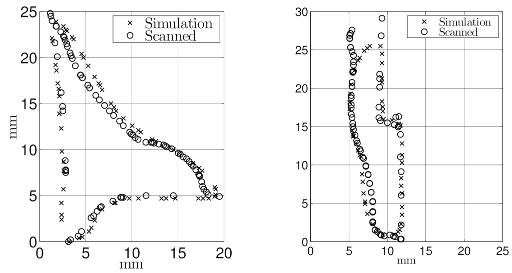


Figure 8. Detailed comparison of the simulated and scanned beads in the cross sections defined in Figure 7.

A simulation is performed with the flow rate 1 ml/s and a rotation speed of 15000 rpm. The nozzle diameter is 0.6 mm and the radius of the rotation 1 mm. The movement speed of the nozzle is zero, in order to focus on the effects of the swirl technique. In Figure 9 snap shots are shown for a time series in the simulation. The spiral pattern of the flow in the air caused by the stresses in the material is clearly visible.

The third and final example is of wire fed additive manufacturing of metals, a process that is used to build or repair structures with complex geometry. A metal wire is continuously fed to the focus spot of a laser beam, caus-

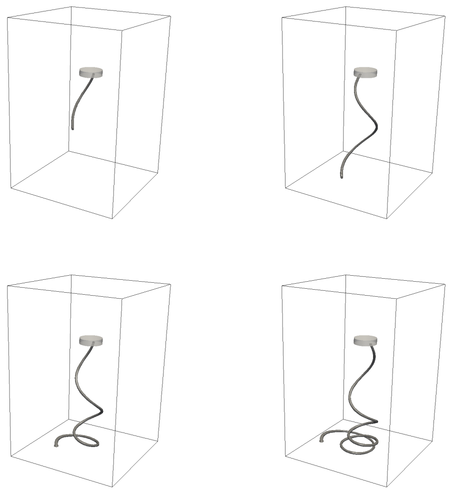

Figure 9. Snapshots of E-swirl simulation at 2 ms (top left), 50 ms (top right), 100 ms (bottom left) and 150 ms (bottom right).

ing the material to melt. The liquid metal then flows onto the substrate surface and eventually solidifies as it cools down.

The direct injection approach with a circular inflow is used for this application. The viscosity is temperature dependent and is calculated from (6) with parameters $\mu_0^T = 1.665\,\mathrm{mPas}$ and $E_A = 48.586\,\mathrm{kJ/mol}$. The heat equation (7) is solved in the whole domain with a conjugate heat transfer solver for the coupled heat transfer between the solid, the liquid metal and the surrounding air. The solidification of the material is modelled by converting fluid cells to solid cells if the temperature falls below the solidification temperature.

A simulation is carried out of a straight single layer. The inlet temperature is 5000 K and the diameter of the inlet is 1.14 mm. The movement speed is 14 mm/s and the flow rate is 0.34 ml/s. In Figure 10 the bead is shown at time 50 ms and at 250 ms, respecively.

The temperature field is significant for the rheology of the liquid metal. The temperature history can also provide input to the micro structure of the final product. In Figure 11 the temperature field at 250 ms is shown in the substrate and the bead, which has been clipped to make the result inside the bead visible. The

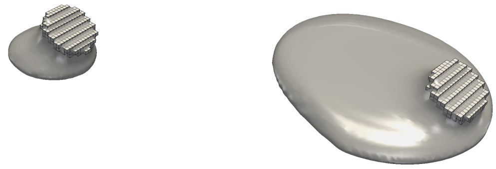

Figure 10. Simulation of wire fed additive manufacturing with bead (contour of $\alpha = 1/2$) and injection cells (solid cubes) at time 50 ms (left) and 250 ms (right).

resulting viscosity in the bead is also shown. As can be expected, the temperature is very high near the injection area but decreases further away. At a certain distance from the injection the temperature is sufficiently low for the metal to solidify. Following from the temperature field, the viscosity is low near the injection but is significantly higher in the cooler parts.

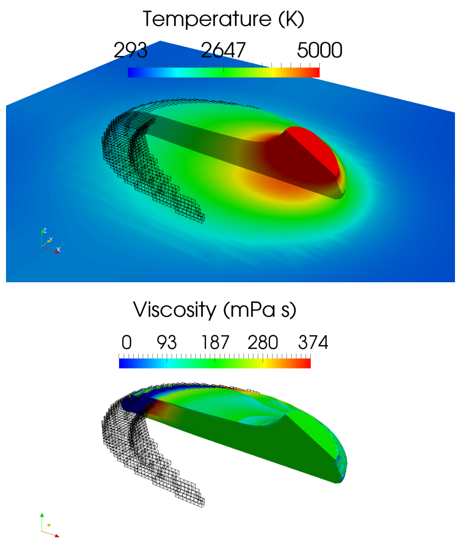


Figure 11. Simulated temperature (top) and viscosity (bottom) for wire fed additive manufacturing. Solidified cells represented with black grid.

## CONCLUSIONS

A numerical framework to simulate various types of dispensing of non-Newtonian fluids has been presented. The framework supports a wide range of applications with injection models for different types of nozzles and a variety of rheology models with different levels of complexity.

Three different example applications have been demonstrated, covering both direct and projected injection models as well as purely viscous rheology models and time dependent viscoelastic stress models. The wide range of the applications included indicates that many different applications could be simulated using the proposed approach. Future work therefore includes expanding the scope of the framework by adding new injection and rheology models.

ACKNOWLEDGEMENTS

This work has been supported in part by the Swedish Governmental Agency for Innovation Systems, VINNOVA, through the FFI Sustainable Production Technology program, and the Compentence Centre for Additive Manufacturing - Metal, CAM$^2$. The support is gratefully acknowledged. Scanned geometries and experimental data for the sealing simulations were provided by Scania trucks.

REFERENCES

1. Thien, N. P. and Tanner, R. I. (1977), “A new constitutive equation derived from network theory”, *Journal of Non-Newtonian Fluid Mechanics*, **2**, 353–365.

2. Larson, R. G. (1988), “Constitutive Equations for Polymer Melts and Solutions”, Butterworth Publishers.

3. Herrchen, M. and Öttinger, H. C. (1997), “A detailed comparison of various FENE dumbbell models”, *Journal of Non-Newtonian Fluid Mechanics*, **68**, 17 - 42.

4. Ubbink, O. and Issa, R. (1999), “A Method for Capturing Sharp Fluid Interfaces on Arbitrary Meshes”, *Journal of Computational Physics*, **153**, 26 - 50.

5. Iske, A. (2004), “Multiresolution Methods in Scattered Data Modelling”, Springer.

6. Mark, A. and Wachem, B. G. M. (2008), “Derivation and validation of a novel implicit second-order accurate immersed boundary method”, *J. of Comput. Physics*, **227**, 6660 - 6680.

7. Brujan, E.-A. (2011), “Cavitation in Non-Newtonian Fluids”, Springer-Verlag.

8. Mark, A., Rundqvist, R. and Edelvik, F. (2011), “Comparison Between Different Immersed Boundary Conditions for Simulation of Complex Fluid Flows”, *Fluid dynamics & materials processing*, **7**, 241-258.

9. Jeyakumar, M., Hamed, M. and Shankar, S. (2011), “Rheology of liquid metals and alloys”, *Journal of Non-Newtonian Fluid Mechanics*, **166**, 831 - 838.

10. Mark, A., Svenning, E. and Edelvik, F. (2013), “An immersed boundary method for simulation of flow with heat transfer”, *International Journal of Heat and Mass Transfer*, **56**, 424 - 435.

11. Mark, A., Bohlin, R., Segerdahl, D., Edelvik, F. and Carlson, J. S. (2014), “Optimisation of robotised sealing stations in paint shops by process simulation and automatic path planning”, *International Journal of Manufacturing Research*, **9**, 4-26.

12. Svenning, E., Mark, A. and Edelvik, F. (2014), “Simulation of a highly elastic structure interacting with a two-phase flow”, *Journal of Mathematics in Industry*, **4**, 7.

13. Mark, A., Ingelsten, S. and Edelvik, F. (2016), “Lay Down Simulation of Viscoelastic Fluids Using the Hybrid Immersed-Boundary Method”, *ICMF-2016 – 9th International Conference on Multiphase Flow, May 22nd – 27th 2016, Firenze, Italy,*.

14. Svensson, M., Mark, A., Edelvik, F., Kressin, J., Bohlin, R., Segerdahl, D., Carlson, J. S. et al. (2016), “Process Simulation and Automatic Path Planning of Adhesive Joining”, *Procedia CIRP*, **44**, 298 - 303.

15. Edelvik, F., Mark, A., Johnson, T. and Carlson, J. (2017), “Math-Based Algorithms and Software for Virtual Product Realization Implemented in Automotive Paint Shops”, ”Math for the Digital Factory”, Springer-Verlag.